Role of SiC substrate surface on local tarnishing of deposited silver mirror stacks

Emna Limam, Vincent Maurice, Antoine Seyeux, Sandrine Zanna, Lorena H Klein, Grégory Chauveau, Catherine Grezes-Besset, Isabelle Savin de Larclause, Philippe Marcus

Preprint version accepted for publication in *Applied Surface Science*
DOI: 10.1016/j.apsusc.2017.12.170

Role of SiC substrate surface on local tarnishing of deposited silver mirror stacks

Emna Limam,[a] Vincent Maurice,[a] Antoine Seyeux,[a] Sandrine Zanna,[a] Lorena H. Klein,[a] Grégory Chauveau,[b] Catherine Grèzes-Besset,[b] Isabelle Savin De Larclause,[c] Philippe Marcus[a]

[a]PSL Research University, CNRS-Chimie ParisTech, Institut de Recherche de Chimie Paris, Physical Chemistry of Surfaces Group, 11 rue Pierre et Marie Curie, 75005 Paris, France

[b]CILAS MARSEILLE, 600 avenue de la Roche Fourcade, Pole ALPHA Sud - Saint Mitre, 13400 Aubagne, France

[c]CNES, Sous-direction Assurance Qualité, Service Technologies, Matériaux et Procédés, 18 Avenue Édouard Belin, 31401 Toulouse, France

Abstract

The role of the SiC substrate surface on the resistance to the local initiation of tarnishing of thin-layered silver stacks for demanding space mirror applications was studied by combined surface and interface analysis on model stack samples deposited by cathodic magnetron sputtering and submitted to accelerated aging in gaseous H_2S. It is shown that suppressing the surface pores resulting from the bulk SiC material production process by surface pretreatment eliminates the high aspect ratio surface sites that are imperfectly protected by the SiO_2 overcoat after the deposition of silver. The formation of channels connecting the silver layer to its environment through the failing protection layer at the surface pores and locally enabling H_2S entry and Ag_2S growth as columns until emergence at the stack surface is suppressed, which markedly delays tarnishing initiation and thereby preserves the optical performance. The results revealed that residual tarnishing initiation proceeds by a mechanism essentially identical in nature but involving different pathways short circuiting the protection layer and enabling H_2S ingress until the silver layer. These permeation pathways are suggested to be of microstructural origin and could correspond to the incompletely coalesced intergranular boundaries of the SiO_2 layer.

Keywords: Mirror layers; protection layers; silver; silicon dioxide; atmospheric corrosion; tarnishing mechanism; surface analysis; ToF-SIMS; XPS; AFM

Introduction

Space telescopes are equipped with mirrors consisting of thin-layered stacks including a reflecting metallic layer and a protection dielectric layer [1-4]. Silver is used as reflecting layer for its highest reflectivity in the visible and lowest emissivity in the infrared [5,6] while SiO_2 [7,8] Al_2O_3 [9,10] Si_3N_4 [11,12] or SiN_x [13-15] overcoats have been developed for confinement of the silver layer and protection from degradation in earth atmosphere. Despite this protection, silver space mirrors are susceptible to local degradation by tarnishing during indoor qualification and storage phases, limiting their long-term environmental durability after satellite assembly and before launching.

Silver sulfide (Ag_2S) is the predominant tarnish product of silver found in indoor atmospheres as a result of corrosion by organosulfur compounds or H_2S pollutants [16-22] and H_2S is the most used corrosive agent to study silver sulfidation in laboratory [23-27]. It has been shown that a H_2S concentration as low as 0.2 ppb is sufficient to initiate silver sulfidation [28]. Degradation studies performed on space silver mirrors mostly addressed the efficiency of the protection layer and the effect of environmental aging on the optical properties [10,15,25,29-31], and more seldom their tarnishing mechanism [32-35].

In a recent work [35], we studied model stack samples consisting of thin silver layers covered by SiO_2 coatings deposited by cathodic magnetron sputtering on SiC, a substrate already in use in light weight all-SiC telescopes assigned to scientific or earth observation missions. These stacks were submitted to accelerated aging in H_2S gas and studied by combined surface and interface analysis using Atomic Force Microscopy (AFM), X-ray Photoelectron Spectroscopy (XPS) and Time-of Flight Secondary Ion Mass Spectrometry (ToF-SIMS). It was shown that local tarnishing is initiated by the formation of Ag_2S columns emerging above the stack surface. Ag_2S growth was promoted at high aspect ratio defects (surface pores) of the SiC substrate as a result from a failing protection by the covering SiO_2

layer. It was proposed that, in the failure sites, permeation channels connect the silver layer to its environment through the deposited protection layer, like observed with silicon dioxide barrier layers on polymer substrates [36-38], and would enable local H_2S entry and Ag_2S growth until eruption at the stack surface.

Here we bring new insight on the improved local resistance to tarnishing observed on a SiC substrate pretreated by chemical vapor deposition so as to suppress the high aspect ratio defects (surface pores) promoting degradation. Model stack samples consisting of thin silver mirror layers covered by SiO_2 overcoats with adhesion interfacial layers were analyzed by AFM, ToF-SIMS and XPS before and after accelerated ageing in gaseous H_2S environment in order to study the beneficial effect of the SiC substrate surface pretreatment.

Experimental

Two types of Boostec® SiC samples (10 x 10 x 1.5 mm) were purchased from Mersen. The samples hereafter denoted SiC were specified to have an optical surface polish with a nominal rms roughness of 4.4 nm. Those hereafter denoted SiC+CVD had one face pretreated by chemical vapor deposition (CVD) at Mersen so as to deposit a high purity SiC layer, ~200 µm thick, in order to suppress surface pores as specified by Mersen. Their nominal rms roughness was 1.2 nm after surface polish.

All layers in the stacks were prepared by cathodic magnetron sputtering using the PACA2M deposition platform installed in clean room at CILAS Marseille [39-41]. The platform is equipped with an *in situ* broadband optical monitoring of the optical performance and deposited thickness [40]. Base pressure and working pressure during deposition were of 10^{-7} mbar and 10^{-3}-10^{-2} mbar, respectively. The deposited stacks consisted of (i) an adhesion interlayer of metallic nickel and chromium, about 10 nm thick, (ii) a silver mirror layer, 100

to 200 nm thick, (iii) an adhesion interlayer[a], and (iv) a dielectric protection layer of silicon dioxide, from 140 to 200 nm thick depending on the targeted optical performance. Prior to deposition, the target cathode surfaces were pretreated by Ar sputtering in order to minimize their surface contamination. After preparation the stack samples were taken out to clean room atmosphere and enclosed in membrane boxes under ambient pressure before shipping to CNRS-Chimie ParisTech for surface and interface analysis and accelerated aging tests.

Accelerated atmospheric aging was performed in gaseous H_2S selected as most corrosive indoor atmospheric agent of silver. The accelerated aging tests were performed at 1000 mbar H_2S and 75°C for 24, 48 and 96 h, like previously described [35]. The sulfurized samples were transferred through air for surface analysis.

AFM imaging was performed in intermittent contact (tapping®) mode in air, using an Agilent 5500 microscope. A silicon cantilever with a resonance frequency in the range 200-400 kHz and a force constant in the range 25-75 Nm^{-1} was employed. The silicon tip had a nominal radius < 10 nm. Sets of images were recorded over areas of 50×50 μm^2, 20×20 μm^2 and 5×5 μm^2 for each sample at different surface locations to ensure for surface homogeneity. Densities were estimated from the local images recorded over 50×50 μm^2 and 20×20 μm^2 areas and extrapolated to 1 cm^2.

ToF-SIMS analysis was performed at a pressure of approximately 10^{-9} mbar with an IonTof 5 spectrometer. For depth profiling analysis, a pulsed 25 keV Bi^+ primary ion source delivering a target current of 1.2 pA over a 100×100 μm^2 area was interlaced with sputtering performed with a 2 keV Cs^+ ion gun delivering 100 nA of target current over a 300×300 μm^2 area. These conditions were reproduced for all samples allowing direct comparison of the relative secondary ions intensities. For chemical imaging, a pulsed 25 keV Bi^+ primary ion source was employed, delivering 0.15 pA of current over a 100×100 μm^2 area analyzed with

[a] Thickness, material and chemical composition of this interlayer cannot be disclosed

a resolution of about 150 nm. Data acquisition and post-processing analyses were performed with the Ion-Spec software.

XPS analysis was performed at an operating pressure of about 10^{-9} mbar with a VG ESCALAB 250 spectrometer calibrated against the reference binding energies (BE) of clean Cu (932.6 eV), Ag (368.2 eV) and Au (84 eV) samples. Survey spectra and high resolution spectra of the C 1s, O 1s, Si 2p, S 2p and Ag 3d core level regions were collected at 90° take-off angle and with a pass energy of 100 and 20 eV, respectively, using an Al Kα monochromatized X-ray source (hν = 1486.6 eV).. Data processing (peak fitting and decomposition) was performed with the Advantage software provided by Thermo Electron, using a Shirley-type background, component peaks defined by BE, Full Width at Half Maximum (FWHM) and Gaussian/Lorentzian envelopes combined at a fixed ratio of 70/30. BEs of the component peaks were corrected with reference to the C 1s peak for -CH_2-CH_2- bonds set at 285.0 eV. Atomic concentration ratios were calculated from the intensities of the component peak assuming a homogeneous semi-infinite material and using the calibrated transmission factors of the spectrometer, Scofield photoionisation cross sections and values of the photoelectron attenuation lengths calculated using the method of Tanuma et al. [42].

Results and Discussion

SiC substrate and stack surface morphology

Figure 1 shows typical AFM topographic images of the bare substrates and stacks for the SiC and SiC+CVD samples. They confirmed that the surface porosity characterizing the SiC substrate and originating from the material production process is suppressed by the CVD surface treatment like specified by the provider. On the SiC substrate (Figure 1(a,b)), the lateral dimensions (0.5-6 µm), depth (0.05-0.4 µm) and density (~1.6×10^6 cm^{-2}) of the surface

pores remain essentially unchanged after deposition of the stacks, showing that the pores remain incompletely filled and that the surface still exhibits high aspect ratio topographic sites as discussed previously [35]. On the SiC+CVD substrate (Figure 1(d)), the pores have been filled by the deposition of the ~200 µm thick CVD SiC film. The images show the presence of polishing grooves with a local depth reaching 3 nm. This is indicative of the subsequent polishing treatment performed by the provider and suppressing all traces of the initial surface pores that may subsist in case of conformal growth of the CVD film. The measured rms roughness is 0.8 nm, in good agreement with the nominal value of 1.2 nm and significantly lower than that (3.7 nm) measured on the SiC substrate (nominal value of 4.4 nm). At higher magnification, a granular morphology characterizes the surface of the SiO_2 protection layer, both on the SiO_2/Ag/SiC (Figure 1(c)) and SiO_2/Ag/SiC+CVD (Figure 1(e,f)) stacks. The grains have lateral dimensions of 50-150 nm on both substrates, as measured from Figure 1(c) and Figure 1(e). This morphology appears compact on both substrates revealing no detectable pores or pinholes of sub-micrometer dimension.

Depth profiling of as-received stacks

ToF-SIMS elemental depth profiles of the as-received SiO_2/Ag/SiC and SiO_2/Ag/SiC+CVD stacks are shown in Figure 2(a) and (b), respectively. The intensities of the selected ions are plotted on a logarithmic scale *versus* sputtering time. Starting from the outer surface, they allow us defining the following five regions (all marked): the protection layer region (using the SiO^- and $^{18}O^-$ ions), the adhesion interfacial layer I_a, the silver mirror layer and the adhesion interfacial layer I_b regions (all three using the Ag^- ions) and the SiC substrate region (using the SiC^- and C^- ions). The I_a and I_b interfacial layer regions can also be defined using their respective ions as reported previously [35].

In the protection layer region, the SiO^- and $^{18}O^-$ ions profiles exhibit plateaus of increasing intensity with in-depth progress on both substrates, confirming on the SiC+CVD

sample the observation made on the SiC sample [35] and suggesting a density of the SiO_2 layer increasing with in-depth progress, i.e. decreasing with on-going deposition from the I_a interface, independently of the presence of SiC surface pores. In this protection layer region, the ions characteristic for the substrate (SiC^- and C^-) and silver layer (Ag^-) are detected at trace level on the SiC+CVD sample. Carbon contamination during deposition and silicium-carbon combination during analysis can be an explanation for the detection of the SiC^- and C^- ions. Silver contamination of the target cathode during deposition of the previous layers could explain the detection of the Ag^- ions. The presence of Ag in the protective SiO_2 layer could also result from photo-enhanced diffusion during deposition promoted by oxygen adsorption on silver, as previously proposed for a TiO_2 protection layer [43]. Still the pronounced decrease in intensity of these ions measured on the SiC+CVD sample compared to the SiC sample appears to be a direct effect of the suppression of the substrate surface pores, as confirmed by the AFM data, and thus of the channels in the protection layer exposing the underlying silver layer and substrate at the surface pores. This conclusion is also supported by the comparison of the profiles of the Cl^-, $^{34}S^-$ and CN^- ions, characteristic of atmospheric contamination by chlorine-, sulfur- and nitrogen-containing pollutants, respectively. Their trace level measured in the protection layer region of the SiC+CVD sample could originate from residual contamination during deposition (except for sulfur which is not detected in the protection layer region). However, the marked increase on the SiC sample is consistent with the presence of penetration pathways (i.e channels), associated with the presence of the substrate surface defects (i.e. pores) and enabling the permeation of the contaminants from the atmosphere [36-38].

Like previously discussed [35], the peak of the Ag^- ions profile in the I_a interfacial region is consistent with the formation of a discontinuous adhesion interlayer forming islands [2,13], possibly as a result of silver diffusion during deposition [43] and promoting the

nucleation of a protection layer of decreased permeability [29,32,44]. This peak is also observed on the SiC+CVD sample, however with a much steeper increase at the approach of the I_a interfacial region. This is consistent with the formation of a sharper interface induced by the suppression of the substrate pores. In the silver layer region, the Ag^- ions profile exhibit a plateau consistent with the formation of a continuous metallic layer. On the SiC+CVD sample, all other ions drop down in intensity as expected but much more than on the SiC substrate. Again, this is consistent with the suppression of the substrate holes and the associated decrease in roughness. Like in the SiO_2 protection layer region, the extremely low intensity level of the Cl^-, C^- and CN^- ions in the silver layer region is indicative of trace level contamination possibly occurring during deposition.

In the I_b interfacial region (NiCr), the Ag^- ions drop down in intensity like expected, which coincides with a peak in the $NiCr^-$ ions profile (not shown here) [35]. The SiC^- and C^- ions increase in intensity until reaching a plateau in the SiC substrate region. Again the intensity increases are steeper on the SiC+CVD sample because of the smoother interface formed after suppression of the substrate pores. In the I_b interfacial region, peaks are observed in the SiO^-, $^{18}O^-$, CN^-, Cl^- and $^{34}S^-$ ions profiles which are better defined on the SiC+CVD sample because of the smoother interface on the pore-free substrate surface. They are indicative of contamination of the substrate surface by oxygen, nitrogen, chlorine and carbon prior to the stack deposition. In the substrate region, the Ag^-, SiO^-, $^{18}O^-$, CN^-, Cl^- and $^{34}S^-$ ions profiles drop down in intensity as expected but much more markedly on the SiC+CVD substrate. This is further evidence for the suppression of the substrate surface pores.

Improved resistance to Ag_2S formation

The XPS survey and Ag 3d core level spectra for the SiO_2/Ag/SiC and SiO_2/Ag/SiC+CVD stacks subjected to accelerated aging in H_2S for 96 h are shown in Figure 3. The survey spectra are characteristic of a silicon dioxide surface contaminated by carbon

and evidence the presence of silver only on the SiC sample (Figure 3(a)). For both samples, the C 1s spectra recorded at high resolution exhibited one major component peak set at 285 eV BE (1.8 eV FWHM) and one minor component peak at 287.4±0.1 eV BE (1.8 eV FWHM) corresponding to -CH_2-CH_2- and C=O and/or O-C=O bonded carbon, respectively, which is typical of oxide thin films exposed to ambient air and contaminated by organic pollutants [45-47]. The high resolution Si 2p spectra could be fitted with one single component peak at 103.2±0.1 BE (1.7 eV FWHM) and the O 1s spectra by one single component peak at 533.1±0.1 eV BE (1.7 eV FWHM), like expected for silicon dioxide [48,49]. The intensity ratio of these components yielded an O/Si atomic ratio of 1.9±0.2 corresponding to the SiO_2 stoichiometry.

The XP Ag 3d core level spectra show two peaks assigned to the $3d_{5/2}$-$3d_{3/2}$ spin orbit doublet. On the SiC sample (Figure 3(a)), the $3d_{5/2}$ and $3d_{3/2}$ components are positioned at BEs of 367.8 and 373.8 eV (0.8 eV FWHM), respectively, which does not allow discriminating the Ag(0) metallic state from the Ag(I) oxidized state. However, the Auger parameter α', calculated from the kinetic energy of the Ag M_4NN Auger transition (1129.6 eV) and binding energy of the Ag $3d_{5/2}$ core level, is 724.8 eV, which is in good agreement with values reported for Ag_2S [50-53] and thus shows a Ag(I) oxidation state. The S 2p region for the SiC sample also supports the formation of Ag_2S with its $2p_{3/2}$-$2p_{1/2}$ spin orbit doublet positioned at BEs of 160.7 and 161.9 eV, respectively, in good agreement with those reported for silver sulfide [50,52,54-57]. As previously discussed [35], these data characterize the formation of Ag_2S columns emerging at the surface of the SiO_2 layer and in contact with the conductive silver layer of the stack through the dielectric protection layer.

On the SiC+CVD sample (Figure 3(b)), the high resolution XPS Ag 3d core level region exhibits a signal undetected in the survey spectra because of its low intensity. Two Ag $3d_{5/2}$-$3d_{3/2}$ spin orbit doublets are resolved. The $3d_{5/2}$ and $3d_{3/2}$ components of the minor

intensity doublet are positioned at BEs of 367.8 and 374.0 eV (1.8 eV FWHM), respectively, in good agreement with those measured on the SiC sample. Consistently, they are also assigned to the formation of Ag_2S columns emerging at the surface of the dielectric SiO_2 layer, but in trace quantity compared to the SiC sample. The $3d_{5/2}$ and $3d_{3/2}$ components of the major intensity doublet are shifted to higher BE at 369.9 and 375.9 eV (1.8 eV FWHM), respectively, which is assigned to an electrical charging effect, as previously observed on the as-received SiC sample prior to sulfidation [35]. This higher BE Ag 3d doublet is thus assigned to the residual presence of silver also at the surface of the dielectric SiO_2 layer but electrically isolated from the conductive mirror layer, so that there is no compensation of the charge during photoelectron emission. This residual contamination by silver of the surface of the as-received stacks is confirmed by the ToF-SIMS depth profiles that show a peak on the Ag^- ions in the very first seconds of sputtering (Figure 2(b)). It most likely occurred in the cathodic magnetron sputtering chamber after deposition of the SiO_2 protection layer. In the Ag $M_{45}NN$ Auger transition region, the signal was below the detection limit precluding the determination of the Auger parameter α' and thus the identification of Ag_2S. Likewise no S $2p_{3/2}$-$2p_{1/2}$ spin orbit doublet could be discriminated from the background on the SiC+CVD sample sulfurized for 96 h, also because of an intensity below the detection limit. Still the sulfidation of these silver surface traces is most likely after accelerated aging in H_2S for 96 h and proven by ToF-SIMS data presented further on.

The Ag/(Si+O) atomic ratio calculated from the component peak intensities is 1.8×10^{-2} for the SiC sample but only 0.1×10^{-2} for the SiC+CVD sample, demonstrating the markedly improved resistance to sulfidation brought by the suppression of the substrate surface pores. If one excludes from the calculation the silver surface contamination of the protection layer of the as-received SiC+CVD sample (higher BE Ag $3d_{5/2}$ and $3d_{3/2}$ components), this ratio drops down to $\sim0.03\times10^{-2}$, i.e. a factor of 1/60 compared to the SiC sample, showing that the

formation of Ag_2S columns emerging at the surface of the protection layer is nearly suppressed in our severe accelerated aging conditions.

Residual local initiation of tarnishing

AFM topographic images of the stacks after 24 h accelerated aging in H_2S are shown in Figure 4. On the SiC sample (Figure 4(a)), local protruding features replace most of the surface pores as judged from their respective densities estimated to ~1.4×10^6 cm^{-2} and ~1.6×10^6 cm^{-2}, respectively, confirming that Ag_2S columns have grown from the silver layer and through the protection layer, locally failing at the substrate pores, to erupt above the protection layer. On the SiC+CVD sample (Figure 4(b)), local protruding features are also observed but with a density reduced by a factor of at least 1/10 as judged from these AFM observations. Their lateral dimensions (0.5-2 µm) and height (0.1-0.3 µm) are also markedly lower that on the SiC sample (0.4-6 µm and 0.1-1 µm, respectively), confirming the markedly improved resistance to the local initiation of tarnishing brought by the suppression of the SiC substrate surface pores. Combined with the XPS data, these AFM data also show that the residual initiation of tarnishing measured on the SiC+CVD sample is local and corresponds to the formation of Ag_2S hillocks protruding from the protection layer surface. It is unclear from these XPS data alone if the Ag_2S hillocks observed correspond to the sulfidation of the silver residual surface contamination and or to the emergence at the surface of Ag_2S columns growing from the silver mirror layer.

ToF-SIMS elemental images (100 × 100 μm^2) of the surface of the stacks after 24, 48 and 96 h accelerated aging in H_2S are shown in Figure 5. They were obtained after removal of the organic carbon contamination from exposure to ambient air by light sputtering of the surface. Superimposed O^-+S^- ions images are displayed with O^- and S^- images color-coded in green and red, respectively (color online). The images for the SiC sample (Figure 5(a)) have been discussed previously [35] and are reproduced here for the sake of comparison. They

show that sulfidation is local and dispersed (S^- ions) and coincides with the presence of defects in the protection oxide layer (O^- ions). With increasing accelerated aging time, the silver sulfide spots corresponding to Ag_2S columns grow in number and size eventually leading to coalescence. On the SiC+CVD sample (Figure 5(b)), not all surface defects of the protection layer are sulfurized which suggests that the protection layer can remain an isolating barrier even if defective at the surface. With increasing accelerated aging time, the density of sulfide spots increases as measured from these $100 \times 100\ \mu m^2$ images, however to much lower extent than on the SiC sample thus confirming a markedly improved resistance to the initiation of local tarnishing. Besides, only a fraction of the observed sulfide spots correspond to the emergence at the surface of Ag_2S columns growing from the silver mirror layer according to the XPS data.

Figure 6 shows the specular reflectance spectra of the stacks prior to and after 24, 48 and 96 h accelerated aging in H_2S. All curves show reflectivity drops at 315 and 375 nm related to plasmon absorption by the Ag layer and by the silicon dioxide protection layer, respectively. The decrease of reflectivity caused by the protection layer and its adhesion layer above 330 nm was estimated to about 3% by comparison of stacks with and without the silicon dioxide overcoat on reference glass and silica substrates. Comparing the as-received SiC (Figure 6a) and SiC+CVD (Figure 6b) samples shows that the gain of specular reflectivity brought by the suppression of the SiC substrate surface pores and associated defects in the deposited stack is about 5%. Accelerated aging in H_2S leads to the failure of the optical performance on the SiC sample as shown by the pronounced loss of reflectivity already observed after 24 h and amplified after 48 and 96 h. Clearly, it is caused by the development the silver sulfide spots corresponding to Ag_2S columns invading the reflective stack. On the SiC+CVD samples, no reflectivity loss is observed after 24 and 48 h of accelerated aging, confirming the markedly improved resistance to sulfidation of the stacks.

For the sample aged for 96 h (and its reference), the reflectivity is lower in the 350-550 nm range owing to some variation of the protection layer thickness of the as received stacks. Above this spectral range, the loss of specular reflectivity is only about 2% with respect to the as-received sample, markedly lower than that measured after aging the SiC sample for 96 h (33%) and even 24 h (7%). The reflectivity of the SiC+CVD sample after 96 h aging is also observed to be higher than that of the SiC sample before aging, showing that the suppression of the SiC substrate surface pores improves the resistance to the initiation of tarnishing as well as the optical properties.

Sub-surface penetration of sulfur and initiation of tarnishing

Comparative ToF-SIMS depth profiles of the SiO^-, minor isotope $^{34}S^-$ and AgS^- ions measured before (0 h) and after 24, 48 and 96 h accelerated aging in H_2S are shown in Figure 7 for the SiO_2/Ag/SiC+CVD stacks. The interfaces are marked for the 24 and 96 h samples with variations that reflect some dispersion of the as received multilayer stacks, mostly of the protection layer thickness. As discussed above, the SiO^- ions profiles are characteristic for the protection layer and for the residual oxide contamination of the substrate surface prior to deposition of the stack. Their steep intensity variations in the I_a and I_b interfacial layer regions are indicative of the sharpness of the interfaces of the stack improved after suppression of the SiC surface pores. After accelerated aging up to 96 h in H_2S, the SiO^- ions profiles are identical showing that the structure of the stack and sharpness of its interfaces are essentially unchanged and thus that very little if any sulfidation took place underneath the protection layer.

Prior to accelerated aging in H_2S, the $^{34}S^-$ ions profile peaks in the I_b interfacial region, which is also indicative of surface residual contamination of the substrate by sulfur, most likely from ambient air, prior to deposition of the stack. No intensity is measured in the protection layer, I_a interfacial and silver layer regions. After 24 and 48 h accelerated aging,

the $^{34}S^-$ ions profiles are identical in the protection layer region. Looking further in-depth, their intensity increases regularly before dropping at zero in the I_a interfacial and silver layer regions. These profiles reveal that sulfur entered and progressed in the protection layer where it accumulated until reaching saturation level because further progress in the stack was blocked by the I_a interfacial and silver layer regions. H_2S has been shown to molecularly adsorb on SiO_2 [58] and it is inferred that, in our accelerated aging conditions where water, that can promote H_2S dissociation is absent, sulfur entered and accumulated in the protection layer as molecular H_2S. The regularly increasing intensities of the measured profiles with in-depth progress in the protection layer are not characteristic for inward solid state diffusion from the outer surface, for which a profile decreasing in intensity should be observed [59]. This suggests the presence of pathways for H_2S penetration in the protection layer and thus the presence of defects, possibly of microstructural origin and corresponding to incompletely coalesced intergranular boundaries of the SiO_2 layer since AFM revealed a granular surface morphology of this layer. These microstructural defects would connect to form the pathways short circuiting the protection layer and enabling H_2S ingress. The regularly increasing intensities of the $^{34}S^-$ ions profile could then be explained by an increasing density of these channels with in-depth progress in the SiO_2 layer. However, this is not supported by the SiO^- ions profiles also regularly increasing with in-depth progress and suggesting an increasing density of the SiO_2 layer. Outgassing of H_2S from the penetrating pathways in the UHV conditions of the ToF-SIMS measurements cannot be excluded.

Figure 7 also shows that the AgS^- ions profile have quite low intensities and peak concomitantly with the $^{34}S^-$ in the interfacial I_b region and/or Ag^- ions profiles in the interfacial I_a region (shown in Figure 2 prior to accelerated aging). The combination of silver and sulfur secondary ions during analysis is a possible explanation. After 24 and 48 h accelerated aging, the intensities of the AgS^- ions are still extremely low but slightly increase

at the extreme surface of the stack and during the first 100-200 seconds of sputtering before vanishing. This is a clear indication that, at this stage of sulfidation, silver sulfide is not yet formed in the silver layer region and in the deeper part of the protection layer, and thus that the formation of Ag_2S columns growing from the silver layer is not yet initiated despite the penetration of sulfur in the SiO_2 layer, in contrast to what occurs in the presence of the SiC substrate pores. The local spots of sulfidation revealed by AFM (Figure 4) and ToF-SIMS imaging (Figure 5) are then those characterized in XPS by higher BE-shifted Ag $3d_{5/2}$-$3d_{3/2}$ doublets and corresponding to the sulfidation of the silver contamination traces initially present at the surface of the stacks after deposition and/or of those present in the bulk of the protection layer and possibly segregating to the surface during accelerated aging performed at 75°C.

After 96 h accelerated aging, both the $^{34}S^-$ and AgS^- ions profiles increase in intensity in all regions of the stacks, including in the I_a interfacial, silver and I_b interfacial layer regions until then unaltered. This shows that sulfidation of the silver mirror layer has been initiated below the protection layer following its exposure to H_2S penetrating through the channels short circuiting the protection layer. The $^{34}S^-$ ions profile shows a peak increase in the interfacial I_b region underneath the silver mirror layer. Ag_2S growing by cationic outward diffusion of Ag^+ ions [60-62], this suggests that short circuits for sulfur penetration underneath the silver layer have been created by the formation of Ag_2S. Porosity has been previously reported to develop in a silver layer following the formation of Ag_2S by cationic transport [63] and it is possible that in our case pores were formed in the silver mirror layer in the vicinity of the sites of local growth of Ag_2S and subsequently connected to open channels for the penetration of sulfur through the silver layer until the interfacial I_b layer.

At this stage (96 h) of accelerated aging, AgS^- ions are detected all throughout the protection layer region (Figure 7). This is consistent with the growth of Ag_2S columns from

the silver layer and until emergence at the surface of the stack as inferred from the XPS data that show a Ag $3d_{5/2}$-$3d_{3/2}$ doublet non shifted in binding energy in contrast to that corresponding to Ag_2S formation at the surface of the protection layer. The growth of these Ag_2S columns is local as confirmed by the ToF-SIMS (Figure 5) data. It has been shown that Ag_2S does not grow as a continuous layer but rather forms local hillocks that coalesce in advanced stages of sulfidation [64-66]. In our case, the growth of Ag_2S as columns results from the presence of the channels enabling the penetration of H_2S through the protection layer and it is local because of the most likely discontinuous distribution of these pathways short circuiting the protection layer. The Pilling-Bedworth ratio for the formation of Ag_2S from metallic silver being 1.65 as calculated from the molar volume of Ag_2S (33.82 cm^3) and Ag (10.27 cm^3), swelling of the silver mirror layer underneath the protection layer can be expected to result from its local sulfidation. This volume increase would generate mechanical stress that could eventually crack the protection layer above. Newly formed cracks, presumably of nanoscale dimensions since not observed by AFM (Figure 4) nor ToF-SIMS imaging (Figure 5), would then open new permeation pathways, promoting the penetration of H_2S in the protection layer and thereby explaining the increased intensity of the $^{34}S^-$ ions profile measured in the protection layer region after 96 h accelerated aging in H_2S.

Conclusions

AFM, XPS and ToF-SIMS measurements were combined in a comprehensive approach to bring new insight on how to improve the pre-launch long-term environmental durability of thin-layered silver stacks supported on light-weight SiC substrates for space mirror applications. Model stack samples consisting of a thin silver layer and a SiO_2 protection overcoat, with adhesion interfacial layers, and deposited by cathodic magnetron sputtering, were submitted to severe accelerated aging in H_2S gas at 1000 mbar and 75°C.

The results show that markedly improved resistance to local tarnishing and preservation of the optical properties is obtained for stacks supported on a SiC substrate pretreated by CVD so as to deposit a ~2 µm thick SiC film. The CVD surface treatment suppresses the surface pores resulting from the bulk SiC material production process and thereby eliminates the high aspect ratio surface sites that are imperfectly protected by the SiO_2 overcoat after the stack deposition, and thus more susceptible to the initiation of tarnishing. As a result the preferential tarnishing mechanisms, involving channels connecting the silver layer to its environment through the protection layer and enabling local H_2S entry and Ag_2S growth as columns until emergence at the stack surface, is shut down and tarnishing initiation by degradation of the silver layer is markedly delayed and optical performance preserved.

After 96 h accelerated aging at 1000 mbar and 75°C, only trace sulfidation was observed on the CVD pretreated samples. It resulted for its majority from the reaction with H_2S of silver contamination traces initially present at or near the surface of the stack from the deposition process. The minority tarnish traces revealed a degradation mechanism, essentially identical in nature to the preferential mechanism with Ag_2S growing as columns through the protection layer, but involving different pathways short circuiting the protection layer and enabling H_2S ingress until the silver layer. These pathways are suggested to be of microstructural origin and could correspond to the incompletely coalesced intergranular boundaries of the SiO_2 layer.

Acknowledgment

Region Ile-de-France is acknowledged for partial funding of the ToF-SIMS and XPS equipment.

References

[1] D.-Y. Song, R. W. Sprague, H. A. Macleod, M. R. Jacobson, Progress in the development of a durable silver-based high-reflectance coating for astronomical telescopes, Appl. Opt. 24 (1985) 1164–1170.

[2] M. R. Jacobson, R. C. Kneale, F. C. Gillett, K. Raybould, J. F. Filhaber, C. K. Carniglia, R. Laird, D. Kitchens, R. P. Shimshock, D. C. Booth, Development of silver coating options for the Gemini 8-m telescopes project, In: Proc. SPIE 3352, 477-502 (1998).

[3] M. Boccas, T. Vucina, C. Araya, E. Vera, C. Ahhee, Protected silver coatings for the 8-m Gemini telescope mirrors, Thin Solid Films 502 (2006) 275–280.

[4] D. A. Sheikh, Improved silver mirror coating for ground and space-based astronomy, In Proc. SPIE 9912, 991239 (2016).

[5] J. M. Bennett, E. J. Ashley, Infrared Reflectance and Emittance of Silver and Gold Evaporated in Ultrahigh Vacuum, Appl. Opt. 4 (1965) 221-224.

[6] N. Thomas, J. Wolfe, UV-shifted durable silver coating for astronomical mirrors, in Optical Design, Materials, Fabrication, and Maintenance, In Proc. SPIE 4003, Optical Design, Materials, Fabrication, and Maintenance, pp. 312-323 (2000).

[7] D.W. Rice, R. J. Cappell, W. Kinsolving, J. J. Laskowski, Indoor Corrosion of Metals, J. Electrochem. Soc. 127 (1980) 891-901.

[8] M. G. Dowsett, A. Adriaens, M. Soares, H. Wouters, V. V. N. Palitsin, R. Gibbons, R. J. H. Morris, The use of ultra-low-energy dynamic SIMS in the study of the tarnishing of silver, Nuclear Instruments and Methods in Physics Research Section B : Beam Interactions with Materials and Atoms 239 (2005) 51-64.

[9] G. Hass, Reflectance and preparation of front-surface mirrors for use at various angles of incidence from the ultraviolet to the far infrared, J. Opt. Soc. Am. 72 (1982) 27-39.

[10] G. I. N. Waterhouse, G. A. Bowmaker, J. B. Metson, Oxidation of a polycrystalline silver foil by reaction with ozone, Appl. Surf. Sci. 183 (2001) 191-204.

[11] J. M. Bennett, J. L. Stanford, E. J. Ashley, Optical constants of silver sulfide tarnish films, J. Opt. Soc. Am. 60 (1970) 224-231.

[12] A. C. Phillips, J. Miller, W. Brown, D. Hilyard, B. Dupraw, V. Wallace, D. Cowley, Progress toward high-performance reflective and anti-reflection coatings for astronomical optics, In Proc. SPIE 7018, 70185A (2008).

[13] J. D. Wolfe, R. E. Laird, C. K. Carniglia, Durable silver-based antireflection coatings and enhanced mirrors, In: Optical Interference Coatings, Vol. 17, OSA Technical Digest Series (Optical Society of America), 115–117 (1995).

[14] J. D. Wolfe, D. M. Sanders, S. Bryan, N. L. Thomas, Deposition of durable wide-band silver mirror coatings using long-throw, low-pressure, DC-pulsed magnetron sputtering, In Proc. of SPIE: Astronomical Telescopes and Instrumentation: Specialized optical developments in astronomy, The International Society for Optics and Photonics, 343-351 (2003).

[15] D. A. Sheikh, S. J. Connell, R. S. Dummer, Durable silver coating for Kepler Space Telescope primary mirror, In Proc. SPIE 7010, 70104E (2008).

[16] C. Leygraf, I. O. Wallinder, J. Tidblad, T. Graedel, *Atmospheric Corrosion, Second Edition*. John Wiley & Sons, Inc.: Hoboken, USA, 2016.

[17] H. A. Ankersmit, N. H. Tennent, S. F. Watts, Hydrogen sulfide and carbonyl sulfide in the museum environment- Part 1, Atmospheric Environment 39 (2005) 695-707.

[18] J. Horvath, L. Hackl, Check of the potential/pH equilibrium diagrams of different metal-sulphur-water ternary systems by intermittent galvanostatic polarization method, Corrosion Sci. 5 (1965) 525-538..

[19] D. Rice, R. Cappell, P. Phipps, P. Peterson, W. Ailor, Indoor atmospheric corrosion of copper, silver, nickel, cobalt and iron. In: Atmospheric Corrosion (W. H. Ailor, Ed.), Wiley: New York, pp. 651-666 (1982).

[20] Y. Fukuda, T. Fukushima, A. Sulaiman, I. Musalam, L. C. Yap, L. Chotimongkol, S. Judabong, A. Potjanart, O. Keowkangwal, K. Yoshihara, M. Tosa, Indoor Corrosion of Copper and Silver Exposed in Japan and ASEAN1 Countries, J. Electrochem. Soc. 138 (1991) 1238-1243.

[21] S. Bouquet, C. Bodin, et C. Fiaud, Relative Infuence of Sulfide and Chloride Compounds on Tarnishing of Silver in Atmospheric Corrosion, CR. Acad. Sci. II 316 (1993) 459-464.

[22] D. Liang, H. C. Allen, G. S. Frankel, Z. Y. Chen, R. G. Kelly, Y. Wu et B. E. Wyslouzil, Effects of Sodium Chloride Particles, Ozone, UV, and Relative Humidity on Atmospheric Corrosion of Silver, J. Electrochem. Soc. 157 (2010) C146-C156.

[23] D. Pope, H. R. Gibbens, R. L.Moss, The tarnishing of Ag at naturally-occurring H2S and SO2 levels, Corrosion Sci. 8 (1968) 883-887.

[24] S. Lilienfeld, C. E. White, A Study of the Reaction Between Hydrogen Sulfide and Silver. J. Am. Chem. Soc. 52 (1930) 885-892.

[25] D. K. Burge, H. E. Bennett, E. J. Ashley, Effect of Atmospheric Exposure on the Infrared Reflectance of Silvered Mirrors With and Without Protective Coatings, Appl. Opt. 12 (1973) 42-47.

[26] S. Kasukabe, Growth mechanism and growth form of Beta-Ag2S whiskers, J. Cryst. Growth 65 (1983) 384-390.

[27] T. E. Graedel, J. P. Franey, G. J. Gualtieri, G. W. Kammlott, D. L. Malm, On the mechanism of silver and copper sulfidation by atmospheric H2S and OCS, Corrosion Sci. 25 (1985) 1163-1180.

[28] D. W. Rice, P. Peterson, E. B. Rigby, P. B. P. Phipps, R. J. Cappell, R. Tremoureux, Atmospheric Corrosion of Copper and Silver, J. Electrochem. Soc. 128 (1981) 275-284.

[29] Fuqua P. D.; Barrie J. D.; Optical properties and corrosion resistance of durable silver coatings. Mat. Res. Soc. Symp. Proc. 555 (1998) 85–90.

[30] C. T. Chu, P. D. Chaffee, C. J. Panetta, P. D. Fuqua, J. D. Barrie, Mixed Flowing Gas Testing of Silver Mirror Coatings, In: OSA Technical Digest (CD), Optical Interference Coatings, TuEPDP5 (2007).

[31] A. Feller, K. Nagaraju, O. Pleier, J. Hirzberger, P. J. Jobst, M. Schuermann, Reflectivity, polarization properties and durability of metallic mirror coatings for the European Solar Telescope, In: Proc. SPIE 8450, 84503U, 2012.

[32] Pellicori S. F. Scattering defects in silver mirror coatings. Appl. Opt. 19 (1980) 3096-3098.

[33] C.-T. Chu, P. D. Fuqua et J. D. Barrie, Corrosion characterization of durable silver coatings by electrochemical impedance spectroscopy and accelerated environmental testing, Appl. Opt. 45 (2006) 1583-1593.

[34] K. A. Folgner, C.-T. Chu, Z. R. Lingley, H. I. Kim, J.-M. Yang, J. D. Barrie, Environmental durability of protected silver mirrors prepared by plasma beam sputtering. Appl. Opt. 56 (2017) C75-C86.

[35] E. Limam, V. Maurice, A. Seyeux, S. Zanna, L. H. Klein, G. Chauveau C. Grèzes-Besset, I. Savin De Larclause, P. Marcus, Local degradation mechanism by tarnishing of protected silver mirror layers studied by combined surface analysis, J. Phys. Chem. B (2017) DOI: 10.1021/acs.jpcb.7b05015.

[36] A.S. da Silva Sobrinho, J. Chaste, G. Dennler, M.R. Wertheimer, Characterization of Defects in PECVD-SiO2 Coatings on PET by Confocal Microscopy. Plasma Polym. 3 (1998) 231-47.

[37] M. Deilmann, M. Grabowski, S. Theiß, N. Bibinov, P. Awakowicz, Permeation mechanisms of pulsed microwave plasma deposited silicon oxide films for food packaging applications. J. Phys. D: Appl. Phys. 41 (2008) 135207.

[38] S. Wilski, J. Wipperfürth, M. Jaritz, D. Kirchheim, F. Mitschker, P. Awakowicz, R. Dahlmann, C. Hopmann, Mechanisms of oxygen permeation through plastic films and barrier coatings. J. Phys. D: Appl. Phys. 50 (2017) 425301.

[39] G. Chauveau, D. Torricini, C. Grèzes-Besset, D. Stojcevski, M. Lequime, PACA2M: magnetron sputtering for 2-meter optics. In Proc. SPIE 8168, 81680P (2011).

[40] M. Lequime, C. Grezes-Besset, G. Chauveau, D. Stojcevski, Optimization of the Manufacturing Strategies of High Quality Coatings into a 2-Meter Optics Magnetron Sputtering Deposition Machine. In 2014 Technical Conference Proceedings, Optical Coatings (September 29, 2014) TechCon2014, Society of Vacuum Coaters (2014).

[41] N. Valette, G. Chauveau, C. Grèzes-Besset, V. Costes, I. Savin de Larclause, K. Gasc, F. Lemarquis, PACA2M Magnetron sputtering silver coating: a solution for very big mirror dimensions, In ICSO 2014 Proceedings, International Conference on Space Optics, Tenerife, Canary Islands, Spain, 7 - 10 October 2014.

[42] S. Tanuma, C. J. Powell, D. R. Penn, Calculations of electron inelastic mean free paths. Surf. Interface Anal. 21 (1993) 165.

[43] K. Chiba, K. Nakatani, Photoenhance migration of silver atoms in transparent heat mirror coatings, Thin Solid Films 112 (1984) 359-367.

[44] Y. Ben Amor, E. M. Sutter, H. Takenouti, M. E. Orazem, B. Tribollet, Interpretation of electrochemical impedance for corrosion of a coated silver film in terms of a pore-in-pore model. J. Electrochem. Soc. 161 (2014) C573–C579.

[45] R. Lindström, V. Maurice, H. Groult, L. Perrigaud, S. Zanna, C. Cohen, P. Marcus, Li-intercalation behaviour of vanadium oxide thin film prepared by thermal oxidation of vanadium metal, Electrochim. Acta 51 (2006) 5001-5011.

[46] B. Tian, J. Światowska, V. Maurice, S. Zanna, A. Seyeux, L. H. Klein, P. Marcus, Combined Surface and Electrochemical Study of the Lithiation/Delithiation Mechanism

of the Iron Oxide Thin-Film Anode for Lithium-Ion Batteries, J. Phys. Chem. C 117 (2013) 21651−21661.

[47] B. Díaz, J. Światowska, V. Maurice, M. Pisarek, A. Seyeux, S. Zanna, S. Tervakangas, J. Kolehmainen, P. Marcus. Chromium and tantalum oxide nanocoatings prepared by filtered cathodic arc deposition for corrosion protection of carbon steel. Surf. Coat. Technol. 206 (2012) 3903–3910.

[48] M. L. Miller, R. W. Linton, X-ray photoelectron spectroscopy of thermally treated silica (SiO2) surfaces, Anal. Chem. 57 (1985) 2314-2319.

[49] S.-H. Jeong, J.-K. Kim, B.-S. Kim, S.-H. Shim, B.-T. Lee, Characterization of SiO2 and TiO2 films prepared using rf magnetron sputtering and their application to anti-reflection coating, Vacuum 76 (2004) 507-515.

[50] V. K. Kaushik, XPS core level spectra and auger parameters for some silver compounds, J. Electron Spectrosc. Relat. Phenom. 56 (1991) 273-277.

[51] N. H. Turner, J. S. Murday, D. E. Ramaker, Quantitative determination of surface composition of sulfur bearing anion mixtures by Auger electron spectroscopy, Anal. Chem. 52 (1980) 84-92.

[52] M. J. Scaini, G. M. Bancroft, J.W. Lorimer, L. M. Maddox, The interaction of aqueous silver species with sulphur-containing minerals as studied by XPS, AES, SEM, and electrochemistry, Geochim. Cosmochim. Acta, 59 (1995) 2733-2747.

[53] H. Kim, Corrosion process of silver in environments containing 0.1 ppm H2S and 1.2 ppm NO2, Mater. Corros. 54 (2003) 243-250.

[54] C. D. Wagner, A. Joshi, The Auger parameter, its utility and advantages: a review J. Electron Spectrosc. Relat. Phenom. 47 (1988) 283-313.

[55] W. Zhang, L. Zhang, Z. Hui, X. Zhang, Y. Qian, Synthesis of nanocrystalline Ag2S in aqueous solution, Solid State Ion. 130 (2000) 111-114.

[56] M. Doriot-Werle, O. Banakh, P. Gay, J. Matthey, P. Steinmann, Tarnishing resistance of silver-palladium thin films, Surf. Coat. Technol. 200 (2006) 6696-6701.

[57] V. Krylova, J. Baltrusaitis, Synthesis and properties of polyamide-Ag2S composite based solar energy absorber surfaces, Appl. Surf. Sci. 282 (2013) 552-560.

[58] A. Travert, O. V. Manoilova, A. A. Tsyganenko, F. Maugé, J. C. Lavalley, Effect of Hydrogen Sulfide and Methanethiol Adsorption on Acidic Properties of Metal Oxides : An Infrared Study, J. Phys. Chem. B. 106 (2002) 1350-1362.

[59] B. Tian, J. Światowska, V. Maurice, S. Zanna, A. Seyeux, L. H. Klein, P. Marcus - Insight into lithium diffusion in conversion-type iron oxide negative electrode from in situ electrochemical and ex situ surface analysis - Journal of Physical Chemistry C 119 (2015) 919-925

[60] C. Wagner, On the nature of the electric conductivity of alpha-silver sulfide. II. Zeitschrift Fur Physikalische Chemie-Abteilung B-Chemie Der Elementarprozesse Aufbau Der Materie 23 (1933) 469-472.

[61] L. S. Darken, Diffusion, mobility and their interrelation through free energy in binary metallic systems, Transactions of the American Institute of Mining, Metallurgical 175 (1948) 184-201.

[62] G. Bonnecaze, A. Lichanot et S. Gromb, Propriétés électrogalvaniques et électroniques du sulfure d'argent b : Domaine d'éxistence, Journal of Physics and Chemistry of Solids 39 (1978) 299-310.

[63] R. C. Ross, R. Sherman, R. A. Bunger, S. J. Nadel, Plasma oxidation of silver and zinc in low-emissivity stacks in 31st Annual Technical Symposium, Sol. Energy Mater. 19 (1989) 55-65.

[64] D. K. Burge, J. M. Bennett, R. L. Peck, H. E. Bennett, Growth of surface films on silver, Surf. Sci. 16 (1969) 1969.

[65] H. E. Bennett, R. L. Peck, D. K. Burge, J. M. Bennett, Formation and Growth of Tarnish on Evaporated Silver Films J. Appl. Phys. 1969, 40, 3351-3360 J. Appl. Phys. 40 (1969) 3351-3360.

[66] A. E. B. Presland, G. L. Price, D. L. Trimm, Hillock formation by surface diffusion on thin silver films, Surf. Sci. 29 (1972) 424-434.

Figure captions

Figure 1 (color online) Top view AFM topographic images of the SiC (a,b,c) and SiC+CVD (d,e,f) substrates*: (a,d) uncoated samples, (b,c,e,f) stack samples prepared by cathodic magnetron sputtering. Δz range is 150 nm (a), 100 nm (b), 25 nm (c,f); 20 nm (e) and 7 nm (d) and color-coded from dark/black to light/white with increasing z (surface height).*

Figure 2 (color online) ToF-SIMS elemental depth profiles of the stacks on the SiC (a) and SiC+CVD (b) substrates and consisting of the silver mirror layer (marked Ag) deposited on the NiCr layer (marked I_b) grown on the SiC substrate and covered by the silicon oxide protection layer (marked Protection) with an interface layer (marked I_a). Selected negative secondary ions are marked.

Figure 3 (color online) XPS survey and Ag3d core level spectra for the stacks on the SiC (a) and SiC+CVD (b) substrates after 96 h accelerated aging in H_2S at 1000 mbar and 75°C.

Figure 4 (color online) Top view AFM topographic images for stacks on the SiC (a) and SiC+CVD (b,c) substrates after 24 h accelerated aging in H_2S at 1000 mbar and 75°C. Δz range is 100 nm (a) and 20 nm (b,c) and color-coded from dark/black to light/white with increasing z (surface height). (c) is an enlarged new image of the local region marked in (b).

Figure 5 (color online) ToF-SIMS elemental images for the stacks on the SiC (a) and SiC+CVD (b) substrates after 24, 48 and 96 h accelerated aging in H_2S at 1000 mbar and 75°C. Superimposed O^-+S^- images are shown with the O^- and S^- ions color-coded in green and red, respectively.

Figure 6 (color online) Specular reflectance spectra for the stacks on the SiC (a) and SiC+CVD (b) substrates before and after 24, 48 and 96 h accelerated aging in H_2S at 1000 mbar and 75°C..

Figure 7 (color online) ToF-SIMS depth profiles of the SiO^-, AgS^- and $^{34}S^-$ ions for the stacks on the SiC+CVD substrate prior to (0 h) and after 24, 48 and 96 h accelerated aging in H_2S at 1000 mbar and 75°C.

Figure 1

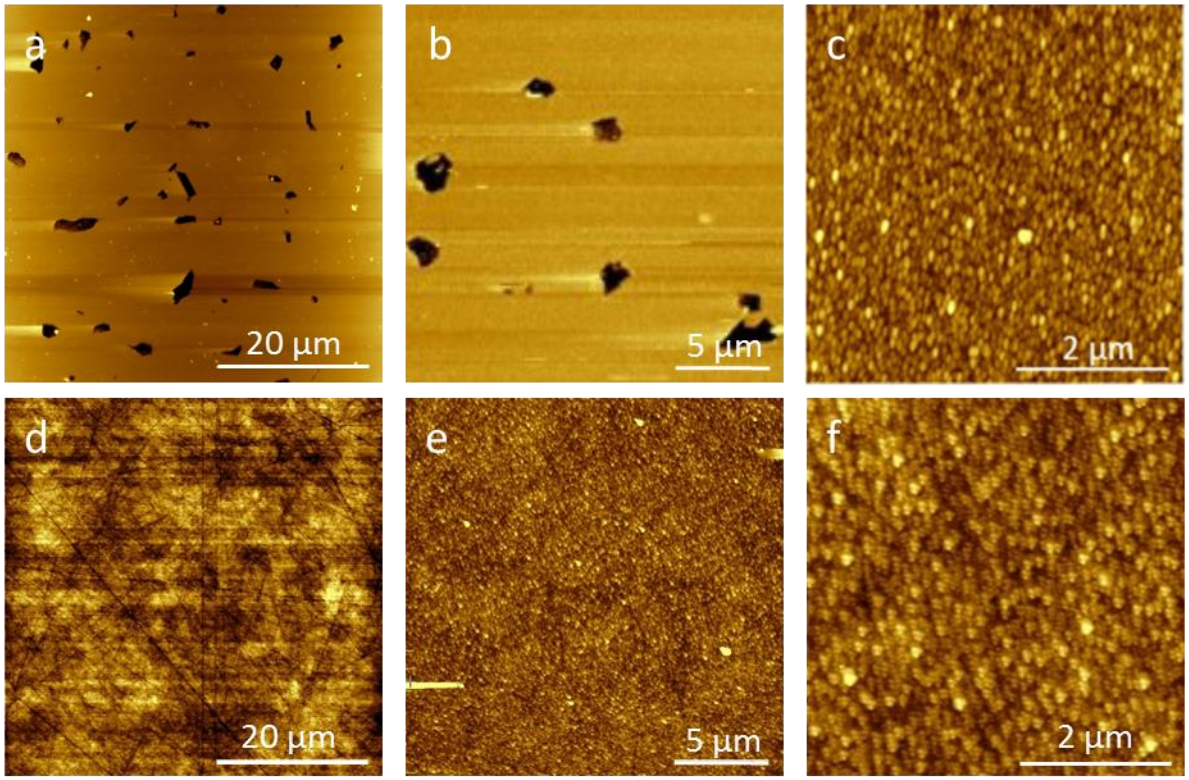

Figure 2

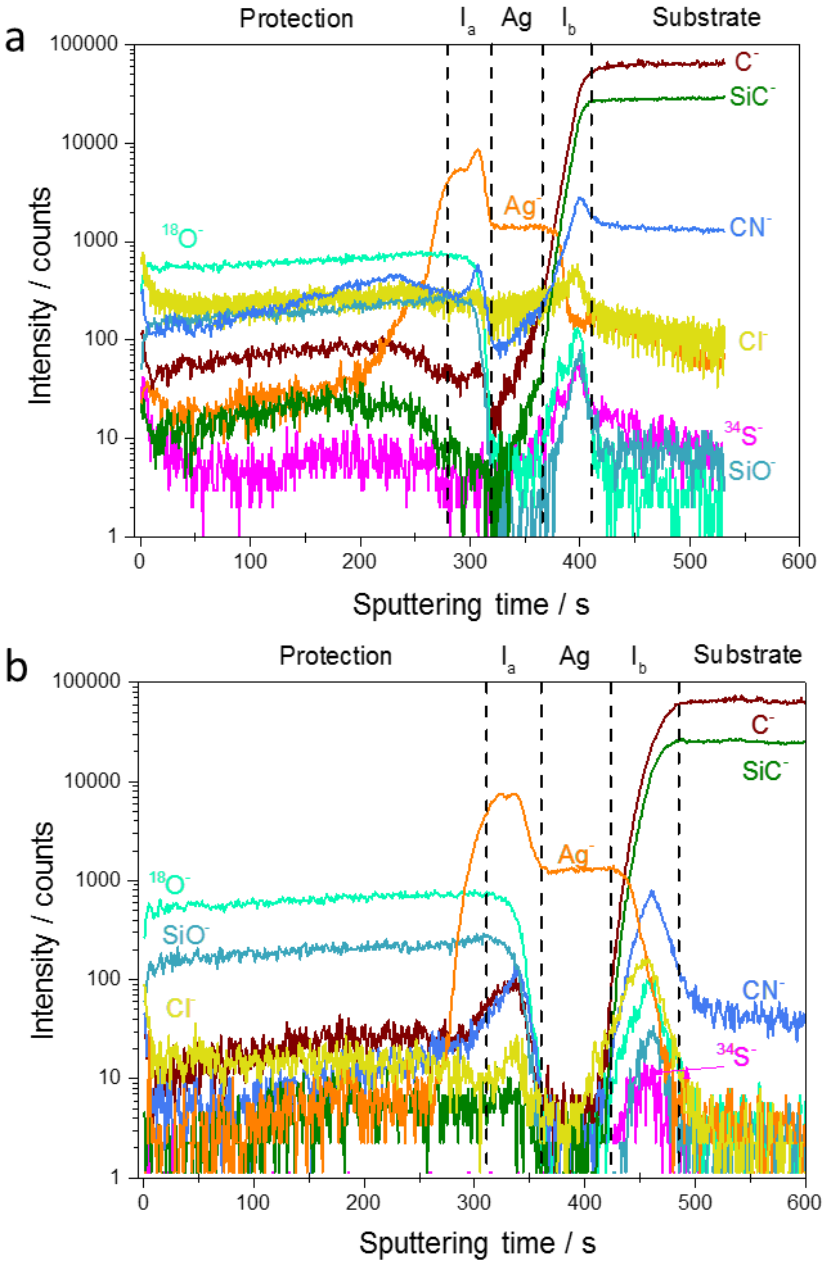
a
Protection
I_a
Ag
I_b
Substrate
Intensity / counts
Sputtering time / s
C^-
SiC^-
CN^-
Cl^-
$^{34}S^-$
SiO^-
Ag^-
$^{18}O^-$
b
Protection
I_a
Ag
I_b
Substrate
Intensity / counts
Sputtering time / s
C^-
SiC^-
Ag^-
$^{18}O^-$
SiO^-
Cl^-
CN^-
$^{34}S^-$

Figure 3

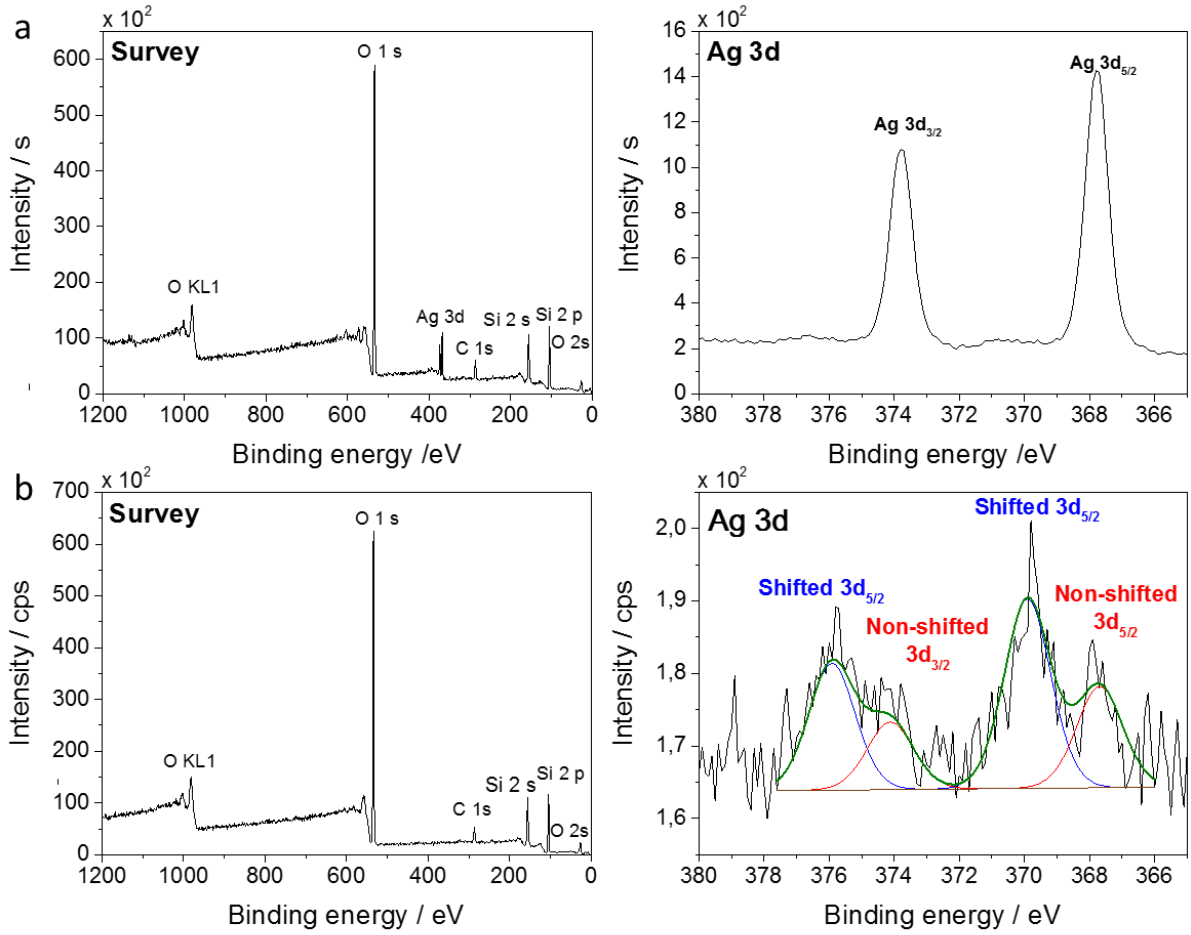
a
x 10^2
Survey
O 1 s
O KL1
Ag 3d
Si 2 s
Si 2 p
C 1s
O 2s
Intensity / s
Binding energy /eV
x 10^2
Ag 3d
Ag 3d5/2
Ag 3d3/2
Intensity / s
Binding energy /eV
b
x 10^2
Survey
O 1 s
O KL1
Si 2 s
Si 2 p
C 1s
O 2s
Intensity / cps
Binding energy / eV
x 10^2
Ag 3d
Shifted 3d5/2
Shifted 3d5/2
Non-shifted 3d3/2
Non-shifted 3d5/2
Intensity / cps
Binding energy / eV

Figure 4

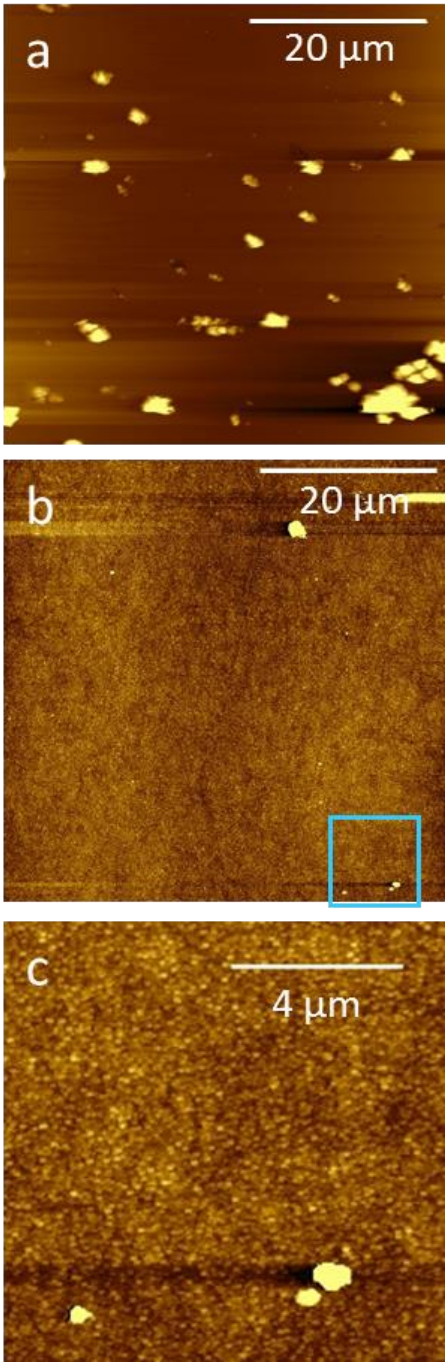

Figure 5

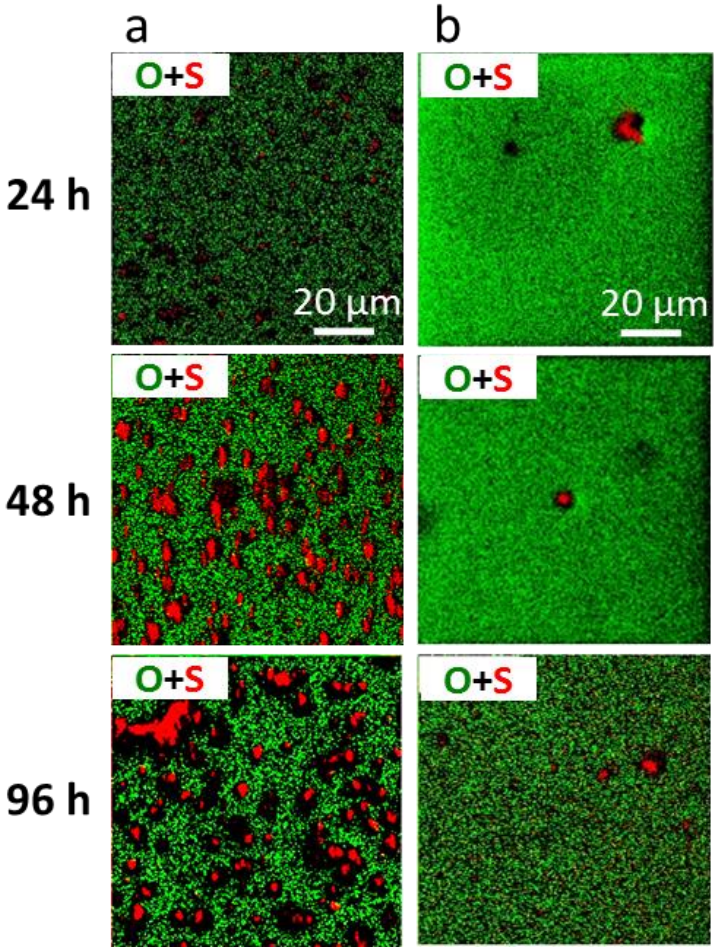

Figure 6

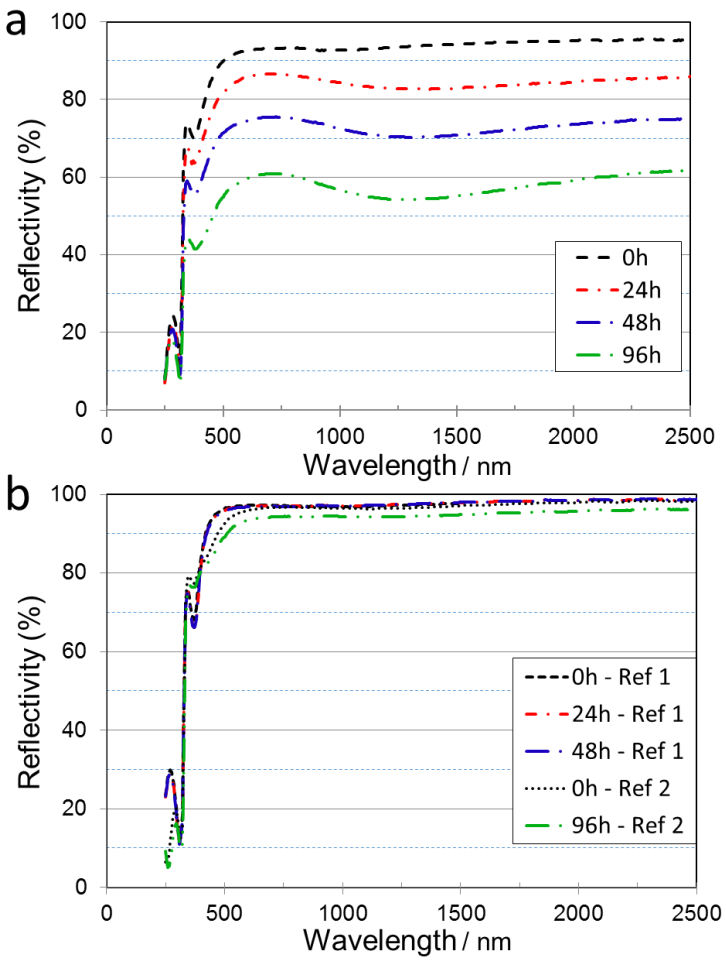
a
Reflectivity (%)
Wavelength / nm
0h
24h
48h
96h
b
Reflectivity (%)
Wavelength / nm
0h - Ref 1
24h - Ref 1
48h - Ref 1
0h - Ref 2
96h - Ref 2

Figure 7

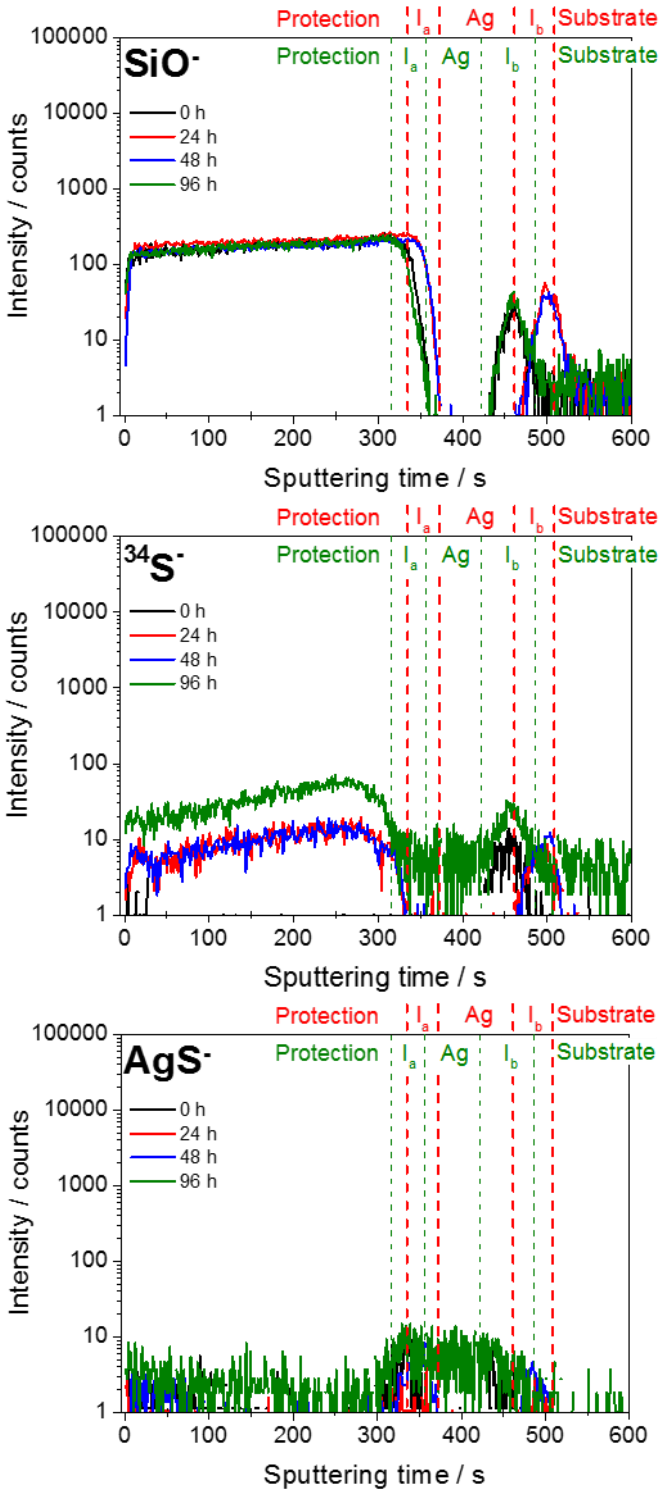
Protection
I_a
Ag
I_b
Substrate
SiO-
^{34}S-
AgS-
0 h
24 h
48 h
96 h
Intensity / counts
Sputtering time / s
100000
10000
1000
100
10
1
0
100
200
300
400
500
600